Hindawi Publishing Corporation
Advances in Optical Technologies
Volume 2008, Article ID 218032, 16 pages
doi:10.1155/2008/218032

Review Article

Three-Dimensional Silicon-Germanium Nanostructures for CMOS Compatible Light Emitters and Optical Interconnects

L. Tsybeskov,[1] E.-K. Lee,[1] H.-Y. Chang,[1] B. V. Kamenev,[1] D. J. Lockwood,[2] J.-M. Baribeau,[2] and T. I. Kamins[3]

[1] *Department of Electrical and Computer Engineering, New Jersey Institute of Technology, Newark, NJ 07102, USA*
[2] *Institute for Microstructural Sciences, National Research Council, Ottawa, Ontario, Canada K1A 0R6*
[3] *Quantum Science Research, Hewlett-Packard Laboratories, Palo Alto, CA 94304, USA*

Correspondence should be addressed to L. Tsybeskov, tsybesko@adm.njit.edu

Received 1 March 2008; Accepted 2 April 2008

Recommended by Pavel Cheben

Three-dimensional SiGe nanostructures grown on Si (SiGe/Si) using molecular beam epitaxy or low-pressure chemical vapor deposition exhibit photoluminescence and electroluminescence in the important spectral range of 1.3–1.6 μm. At a high level of photoexcitation or carrier injection, thermal quenching of the luminescence intensity is suppressed and the previously confirmed type-II energy band alignment at Si/SiGe cluster heterointerfaces no longer controls radiative carrier recombination. Instead, a recently proposed dynamic type-I energy band alignment is found to be responsible for the strong decrease in carrier radiative lifetime and further increase in the luminescence quantum efficiency.

1. INTRODUCTION

Optical interconnects in the form of fiber optics have been used for many years in different long-distance communication applications [1, 2]. With the microprocessor clock speed approaching 10 Gbps, optical interconnects are now being considered for board-to-board and on-chip technology as an alternative to metal wires with their unavoidable RC delay, significant signal degradation, problems with power dissipation, and electromagnetic interference [2–5]. Two major avenues toward optical interconnects on a chip comprise the hybrid approach with III-V optoelectronic components densely packaged into complementary metal-oxide semiconductor (CMOS) architecture [6–9] and the all-group-IV (e.g., Si, SiGe, SiGeC, etc.) approach with the all major components, for example, light emitters, modulators, waveguides, and photodetectors, monolithically integrated into the CMOS environment [10]. There have been great efforts over the past several decades to obtain technologically viable and efficient light emission from group-IV materials. In the visible spectral region, the main emphasis has been on porous silicon [11–13] and other Si nanostructured systems such as silicon/silicon dioxide superlattices [14–17] and silicon nanoprecipitates in silicon dioxide [18, 19]. In the near infrared spectral region, materials and systems such as erbium in silicon [10, 20], silicon/germanium quantum wells [21, 22], and, more recently, iron disilicide [23] offer potentially useful routes. However, no approach has so far been applied commercially. The reasons for this are the lack of a genuine or perceived compatibility with conventional CMOS technology, the long carrier radiative lifetime in Si-based nanostructures, and, especially in the case of near-infrared emitters, the high thermal quenching leading to extremely poor room-temperature luminescence efficiencies [10].

In the 1990s, an interesting form of semiconductor nanostructure, namely, the three-dimensional (3D) self-assembled system produced by the Stranski-Krastanov or cluster-layer, growth mode in lattice mismatched materials, has been demonstrated [24, 25]. In the case of 3D Si/SiGe nanostructures (NSs), the growth of mostly dislocation-free samples has successfully been achieved using both molecular beam epitaxy (MBE) and chemical vapor deposition (CVD) [26–31]. It has been shown that the nonplanar geometry is mainly responsible for the significant increase of the critical layer thickness in 3D Si/SiGe NSs grown on Si [28, 29]. It has also been found that compared to planar Si/SiGe quantum wells (QWs), the photoluminescence (PL) and electroluminescence (EL) quantum efficiency in 3D Si/SiGe NSs is higher, especially at temperatures $T > 50$ K

[32–35]. Despite many successful demonstrations of PL and EL in the spectral range of 1.3–1.6 μm, which is important for optical fiber communications, the proposed further development of 3D Si/SiGe NS-based light emitters was discouraged by several studies confirming a type-II energy band alignment at Si/SiGe heterointerfaces [36–40], where the spatial separation of electrons (located in Si) and holes (localized in SiGe) was thought to make carrier radiative recombination very inefficient. Later, it was also shown that 3D Si/SiGe NSs exhibit an extremely long (of the order of 10^{-2} seconds) luminescence lifetime [41], which is of the order of a million times longer than those found in III-V semiconductors. In addition, single crystal Si and Ge are indirect band gap semiconductors and it has been declared that since carrier radiative recombination is an indirect process in these materials, in both real and reciprocal space, this process should be extremely inefficient. Thus, according to this analysis, 3D SiGe NSs cannot be used to achieve efficient and commercially valuable light emitting devices.

In this review paper, we show that despite the fact that bulk Si and Ge are indeed indirect band gap semiconductors and that the Si/SiGe heterointerface most likely exhibits type-II energy band alignment, it is still possible to obtain conditions favorable for efficient carrier radiative recombination. We demonstrate that the recent revised understanding of basic physics in such systems has already helped to achieve nearly constant luminescence intensity at temperatures 4 K < T < 250 K, and that the radiative carrier recombination lifetime can successfully be reduced from 10^{-2} second to 10^{-7} seconds, which is only ~10 times longer compared to those found in direct band gap III-V semiconductors.

2. GROWTH AND STRUCTURAL PROPERTIES OF Si/SiGe THREE-DIMENSIONAL NANOSTRUCTURES

The standard approach to the fabrication of a 3D Si/SiGe NS, which for most experiments discussed here is a multilayer Si/SiGe cluster system, is based on the sequential physical sputtering of Si and Ge (SiGe) in MBE or the thermal decomposition of SiH_4 and GeH_4 in CVD at a temperature in the range T = 550–650°C. At that temperature, both a high Ge solid solubility in Si as well as strain induced SiGe interdiffusion due to the ~4% lattice mismatch between Si and Ge are important. The MBE growth provides better control over the average SiGe cluster composition, although, because of interdiffusion during growth, the composition is not uniform within the cluster volume [42–45]. Figure 1 shows typical transmission electron micrographs (TEMs) together with a summary of analytical TEM studies confirming both the 3D geometry of the SiGe NSs and the complex atomic composition. In general, SiGe cluster growth commences with the spontaneous development of a $Si_{1-x}Ge_x$ planar, <1 nm thick, wetting layer where x varies, mainly due to uncontrolled SiGe interdiffusion. With the further influx of Ge and Si, the growth mode then switches from two dimensional (a layer) to 3D (a cluster), which helps release some of the lattice-mismatch induced strain [44]. The fully grown 3–10 nm high and initially nearly pyramidal-shaped SiGe clusters have a Ge-rich (~50% depending on the Ge flux) core, although the exact final cluster shape and composition strongly depends on the fabrication conditions [45]. If the SiGe cluster is covered by a Si cap, the initial pyramid-like cluster top is smoothed out (Figure 1(a)), and the capping Si layer is locally strained, mostly near the top of the SiGe cluster. In multilayer Si/SiGe cluster samples, this strain field propagates in the growth direction, and it induces vertical SiGe cluster self-ordering (Figure 1(a)). Detailed structural analysis also indicates that the Si in the valleys between SiGe clusters is slightly compressed [30, 44]. To summarize, buried SiGe clusters with the highest Ge composition of near 50% in the middle of the clusters are surrounded by Si, which is tensile strained above each cluster and compressed laterally between clusters to maintain a low overall strain. Each SiGe cluster consists of $Si_{1-x}Ge_x$ crystalline alloys with x increasing toward the cluster center [43–45]. Thus, despite being fully crystalline alloys, 3D Si/SiGe NSs with a high (~50%) Ge atomic concentration exhibit significant embedded strain and compositional disorder [46]. These conclusions regarding the structural properties of 3D Si/SiGe NSs are critically important in understanding their optical characteristics and light-emitting properties.

3. OPTICAL PROPERTIES OF Si/SiGe THREE-DIMENSIONAL NANOSTRUCTURES

In a system with strong selection rule relaxation, quasidirect carrier recombination is possible, and it should provide a higher PL quantum efficiency compared to that in an indirect band gap semiconductor, for example, single crystal Si and Ge. In fact, many PL measurements in SiGe bulk alloys and Si/SiGe NSs reveal a significantly enhanced intensity ratio between no-phonon (NP) luminescence and phonon-assisted luminescence, as shown in Figure 2(a). On the other hand, in undoped bulk crystalline Si (c–Si), the NP PL line intensity is negligible compared to the transverse optical (TO) and transverse acoustic (TA) phonon-assisted radiative transitions (see Figure 2(b)). Thus, systematic studies of the PL spectra in 3D $Si/Si_{1-x}Ge_x$ NSs with control over the average Ge atomic concentration x provide very important information regarding changes in the carrier recombination mechanism (e.g., selection rule relaxation, conduction and valence band alignment, etc.) as x increases from 0 (c–Si) to ~55%.

Figure 3(a) compares PL spectra in MBE samples with x = 0.096, 0.16, and 0.53. In addition to PL related to c–Si, we observe for x = 0.096 relatively narrow PL bands at 1.05 and 1.11 eV (Figure 3(a)) attributed to NP and TO phonon PL bands in Si-rich SiGe alloys [33–35, 47, 48]. Note that these PL bands are in the vicinity of c–Si luminescence, and that the intensities of these two sets of PL bands are comparable. Therefore, we conclude that a small amount of Ge (<10%) slightly reduces the SiGe band gap and mainly relaxes selection rules, increasing the ratio of NP/TO PL band intensities. The observed broadening of these two PL bands, compared to c–Si related PL, is, apparently, due to the composition disorder resulting from the introduction of substitutional Ge atoms (~10%) into the c–Si matrix.

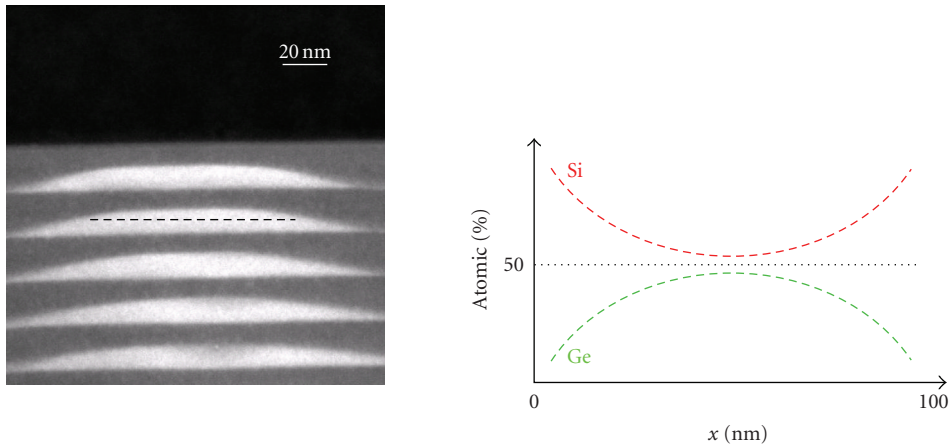

FIGURE 1: (a) Transmission of electron micrograph showing a cross-section of an MBE grown, vertically self-aligned Si/SiGe cluster (or 3D) multilayer structure. (b) Schematic showing typical Si and Ge atomic concentrations within an SiGe cluster measured along a horizontal axis running through the middle of the cluster (see the dashed line in Figure 1(a)).

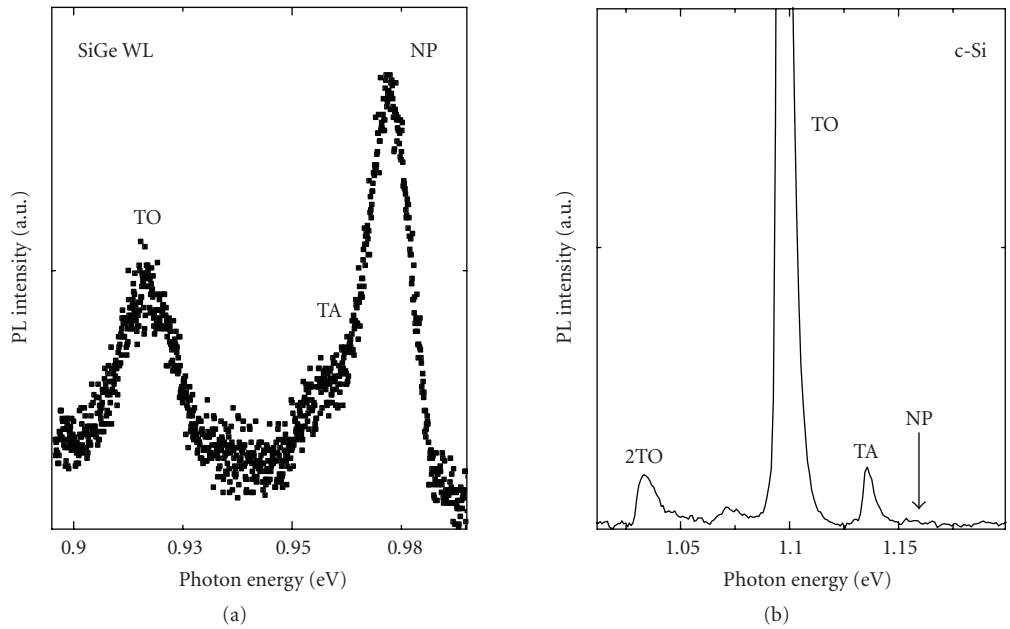

FIGURE 2: Comparison between low temperature ($T = 4$ K) PL spectra in (a) an SiGe wetting layer with ~20% Ge concentration and (b) undoped crystalline Si (c–Si). Note the dramatically different intensity ratios between the NP and TO phonon PL lines of each sample.

Increasing the average Ge composition within $Si_{1-x}Ge_x$ clusters up to $x = 0.16$ results in significant changes in the PL spectrum (Figure 3(b)). An intense PL band peaked at 0.95 eV has appeared, showing an effective SiGe band gap reduction of ~150 meV compared to c–Si. This broad and featureless PL band with a full width at half maximum (FWHM) of ~70 meV indicates a much stronger compositional disorder compared to 3D Si/SiGe NC samples with $x = 0.096$.

The PL spectrum in the samples with an average Ge composition close to 53% (Figure 3(c)) depicts a broad feature with a major PL peak centered at a photon energy of 0.75 eV, and this peak energy is close to the band gap of crystalline Ge (c–Ge) at 4 K [49]. A second PL peak is found at ~0.85 eV. Such samples have the highest PL quantum efficiency as compared to other samples with lower x values. Both PL bands are quite broad, most likely due to compositional disorder, which is in an agreement with the Raman scattering measurements (discussed below).

In contrast to MBE grown samples, CVD growth of 3D Si/SiGe NSs does not provide precise control over the Ge atomic composition, and, most likely, it produces more Si/SiGe interdiffusion at heterointerfaces [42–44, 50]. This is well reflected in PL spectra, where no fine structure has been

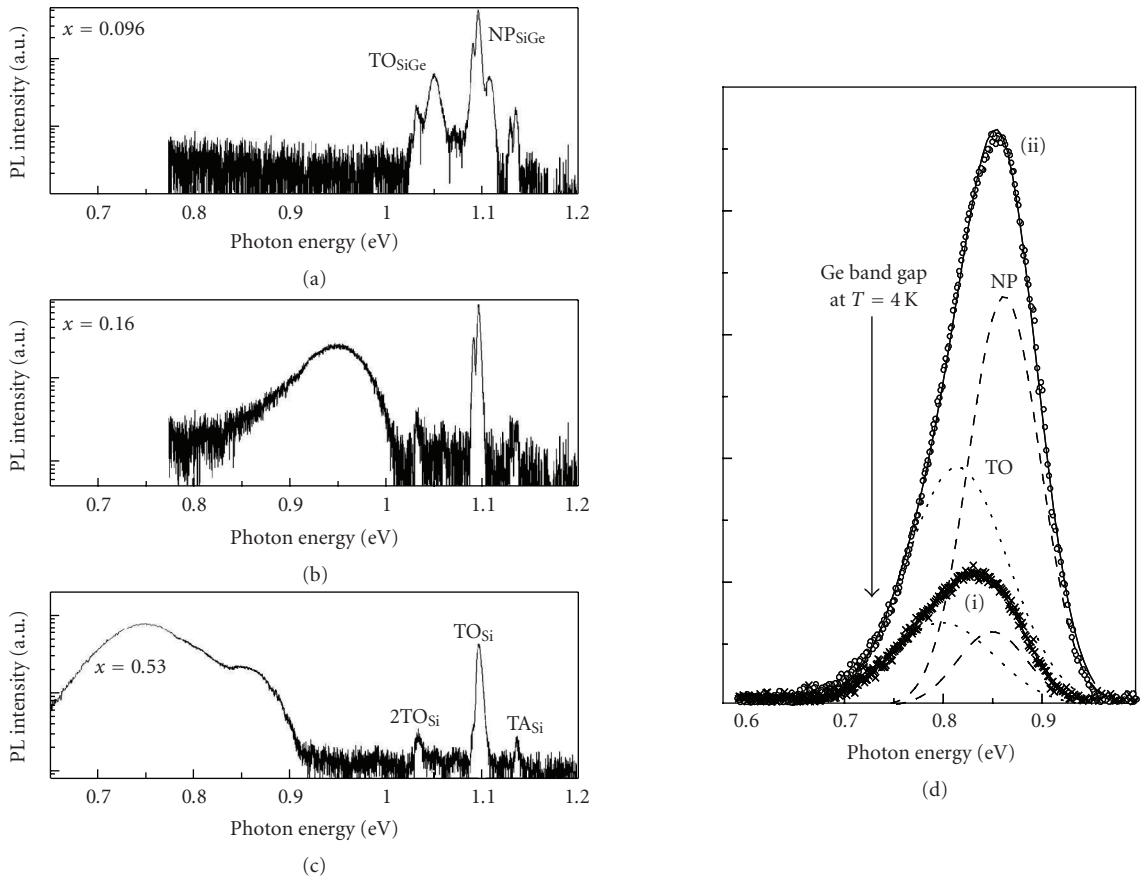

FIGURE 3: (a) Low temperature ($T = 4$ K) PL spectra in (a) MBE grown $Si/Si_{1-x}Ge_x$ 3D NSs with the indicated average Ge atomic concentration x and (d) in Si/SiGe 3D NSs grown by CVD. The characteristic phonon-assisted transitions are indicated. PL spectra in CVD samples show a strong spectral shift toward higher photon energy when the excitation intensity is increased by approximately 5 times from trace (i) to trace (ii) (note the linear intensity scale).

found (see Figure 3(d)). However, the broad and asymmetric PL peak is well fitted by two Gaussian bands often identified as the NP and TO phonon lines [46, 47] that are separated by ~48 meV, which is close to the energy of characteristic SiGe phonons. Thus, there is at least a qualitative similarity between PL spectra in MBE and CVD grown 3D Si/SiGe NSs.

Figure 4 summarizes the PL intensity as a function of excitation intensity in MBE samples having different average Ge atomic concentrations. The same linear dependence (on a log-log plot) for PL associated with c–Si and a sublinear (close to square root) dependence for PL associated with a Ge-rich SiGe cluster core has been found in nearly all 3D Si/SiGe NSs grown by both CVD and MBE [35, 51–53].

Studies of the PL temperature dependence show that at low temperatures the PL intensity is nearly temperature independent. At higher temperatures the PL intensity drops exponentially, and the activation energies of PL thermal quenching are shown in Figure 5. There is a clear correlation between the Ge composition in $Si_{1-x}Ge_x$ 3D nanostructures and the PL intensity temperature dependence. For samples with a low ($x = 0.096$) Ge composition, the activation energy E_a is ~10 meV, and the PL has almost vanished by 40 K. This result could be explained by the thermal dissociation of a nearly free exciton: a localization mechanism associated with SiGe stochiometric fluctuations has been proposed in [53–55]. Figure 4(a) shows that the PL intensity as a function of the excitation intensity is linear (again, on a log-log scale), and that is consistent with the assumption of nearly free exciton PL.

In samples with a higher ($x = 0.16$) Ge composition, the activation energy of PL thermal quenching is increased and the PL is observable up to ~100 K (Figure 5(b)). The broad PL band observed at 0.95 eV for the $Si/Si_{1-x}Ge_x$ sample of $x = 0.16$ exhibits an activation energy of ~25 meV, which combined with a sublinear dependence in PL intensity as a function of excitation intensity (Figure 4(b)) is in contrast with the $x = 0.096$ sample. This observation suggests that the nonequilibrium carriers are spatially localized and that Auger recombination contributes to the overall recombination mechanism even at very low (~100 mW/cm^2) excitation intensity [54, 55]. Most likely, in 3D $Si/Si_{1-x}Ge_x$ NSs with $x = 0.16$, the carriers (possibly holes) are localized within 3D SiGe quasiwells.

In 3D $Si/Si_{1-x}Ge_x$ nanostructures with $x = 0.53$, the PL spectrum contains two bands peaked at 0.85 eV and 0.75 eV (Figure 3(c)). There are no characteristic phonons in the

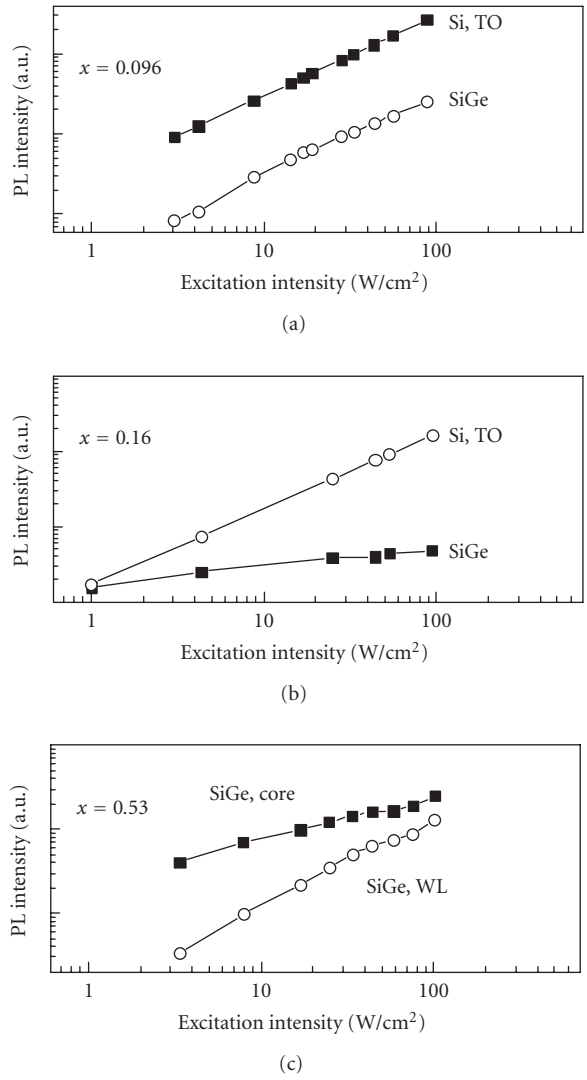

Figure 4: The PL intensity as a function of excitation intensity in MBE grown $Si/Si_{1-x}Ge_x$ 3D NS samples with the indicated average Ge concentration x. The PL bands associated with the cluster core, wetting layer (WL), and characteristic TO phonons are indicated.

Si/SiGe system having an energy of ~100 meV, and it is thus reasonable to assume that the observed PL bands are associated with carrier recombination within two different regions of the 3D SiGe nanostructures. The PL band peaked at 0.85 eV has almost the same PL quenching activation energy (~20 meV) as in the sample with $x = 0.16$, while the PL intensity as function of excitation intensity is linear over a wide range of excitation intensities. The second PL band peaked at 0.75 eV has an activation energy of ~60 meV (Figure 5(c)) and is nearly temperature independent up to 100 K. Because of its high quantum efficiency, it can be monitored almost up to room temperature. This data suggests that 3D $Si/Si_{1-x}Ge_x$ nanostructures with $x = 0.53$ contain coupled subsystems with different (lower and higher) Ge concentrations. It is quite possible that a spatial localization of electron-hole pairs within 3D regions of higher Ge concentration and thus having a lower band gap could be responsible for the observed sublinear excitation dependence of the PL band at 0.75 eV (Figure 4(c)). The remaining 3D regions with a lower Ge concentration (e.g., having a higher band gap) have a lower carrier concentration and the PL band (peaked at 0.85 eV) exhibits a liner excitation dependence.

A continuous shift of the PL band from ~1 to 0.75 eV has been found previously in SiGe alloys with increasing Ge concentration [56]. Instead, in these 3D $Si/Si_{1-x}Ge_x$ samples with a Ge concentration higher than 50%, a simultaneous threshold-like appearance of two clearly resolved PL peaks at 0.85 and 0.75 eV is observed. This suggests that Ge segregation might take place as x increases up to ~0.5. Since the PL peak at 0.75 eV essentially matches the value of the band gap in pure c–Ge, we propose that such a segregation results in a Ge-rich core within an SiGe shell forming the 3D $Si/Si_{1-x}Ge_x$ NSs embedded within a pure Si matrix.

The PL thermal quenching observed in 3D $Si/Si_{1-x}Ge_x$ samples grown by MBE could be associated with different mechanisms. As mentioned earlier, the activation energies of the PL thermal quenching in samples with $x = 0.096$ and $x = 0.16$ are close to the observed exciton binding energy in SiGe alloys and $Si/Si_{1-x}Ge_x$ nanostructures [53–57]. In samples with $x = 0.53$, a greater activation energy could be attributed to carrier diffusion from a 3D potential well. This assumption is justified by the expected type-II band alignment in SiGe nanostructures with a deep (>100 meV) potential well for holes and a relatively small potential barrier for electrons [38, 40, 41]. In this model, phonon-assisted carrier tunneling can produce the observed ~60 meV activation energy for thermal quenching of the PL intensity. The PL intensity behavior as a function of temperature in CVD grown samples is more complex and will be discussed later.

In 3D Si/SiGe NSs, the PL properties strongly correlate with the sample structural properties, and Raman scattering under excitation conditions similar to PL measurements has been shown to be a very informative characterization technique [35]. In fact, in SiGe materials and systems, Raman spectroscopy is a unique characterization technique due to the multimodal nature of Raman scattering from optical phonons in SiGe, which reveals all three major vibrational modes known, respectively, as the Si–Si vibration at ~500 cm^{-1}, the Si–Ge vibration at ~400 cm^{-1}, and the Ge–Ge vibration at ~300 cm^{-1} (see Figure 6, e.g.). In addition, Raman phonon spectroscopy is a very sensitive probe of global and local embedded strain and of compositional and structural disorder. Figure 6 compares Raman spectra for MBE samples of different Ge composition. In $Si_{1-x}Ge_x$ clusters with $x = 0.096$, an intense optical phonon Raman signal associated with Si–Si vibrations is observed at ~520 cm^{-1} together with a weaker feature at ~300 cm^{-1} related to second-order scattering from Si acoustic phonons [58]. No significant Raman peaks related to Ge–Ge vibrations at ~290 cm^{-1} and Si–Ge vibrations at ~420 cm^{-1} [59] and to an amorphous Si phase at ~480 cm^{-1} [60] were found in this or the $x = 0.16$ sample (see Figure 6, noting that the intensity axis has a log scale).

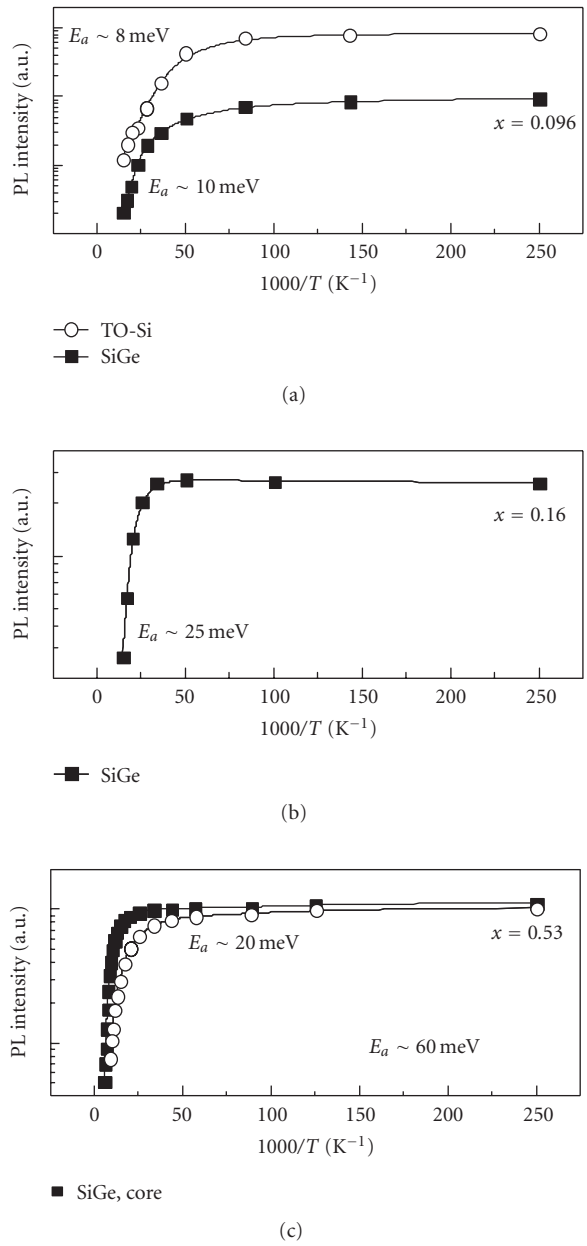

FIGURE 5: The PL intensity temperature dependence in MBE grown $Si/Si_{1-x}Ge_x$ 3D NS samples with the indicated average Ge concentration x measured for different PL bands. Figure 5(c) compares the PL intensity temperature dependencies measured for PL bands with peaks at 0.75 eV (SiGe core) and 0.85 eV.

A further increase in Ge composition to $x = 0.53$ in 3D $Si_{1-x}Ge_x$ NSs produces strong Raman signals at ~290 cm^{-1} (related to Ge–Ge bonds) and at ~420 cm^{-1} (related to Si–Ge bonds), as shown in Figure 6(c). Using a short wavelength photoexitation (458 nm) and multilayer Si/SiGe 3D samples, the Raman signal from the Si substrate is minimized (see Figure 7). In addition to the major vibrational modes indicated in Figure 7(a), a doublet near 520 cm^{-1} related to compressed (~522 cm^{-1}) and strained (~507 cm^{-1}) Si is observed (see Figure 7(b)). The spectrum also exhibits weak and broad (background) Raman peaks in the vicinity of 480–490 cm^{-1} and 250 cm^{-1} related to disordered phases of Si and Ge, respectively. Thus, despite the absence of purely amorphous Si and Ge phases in these 3D nanostructured fully-crystalline alloys, compositional disorder and strain-induced lattice distortion combine to produce similar effects in the Raman spectrum.

4. POLARIZED RAMAN SCATTERING IN Si/SiGe THREE-DIMENSIONAL NANOSTRUCTURES

In addition to conventional inelastic light scattering spectroscopy, polarized Raman scattering provides information on Raman scattering intensity as a function of polarization angle. The result is presented employing polar plots and has been shown to be an informative tool for the analysis of local embedded strain in 3D Si/SiGe NSs with larger dome-shaped SiGe clusters grown on Si (100) substrates [61]. In these measurements, the incident light is usually polarized in the plane of the incident and scattered light, and polarization of the scattered light is analyzed using a thin-film polarizer that can be rotated through 360°.

Figure 8 shows angular Raman polarization diagrams for three different alloy vibrational modes (Si–Si at 520 cm^{-1}, Si–Ge at 415 cm^{-1}, and Ge–Ge at 298 cm^{-1}) for multilayer dome/island samples, as well as the Raman polarization dependence for the Si–Si vibration at 520 cm^{-1} measured in ⟨100⟩ oriented single-crystal Si as a reference. The observed angular dependencies in the polar plots of the Ge–Ge and Si–Ge Raman mode intensities are nearly identical to that in a ⟨100⟩ Si single crystal. However, a quite different behavior is observed in the Raman polarization dependence for the Si–Si vibration at ~519 cm^{-1}.

These different results for the Si–Si mode are emphasized in Figure 8(b), where the Raman spectrum collected at 70° exhibits a major Raman peak at ~520 cm^{-1} slightly shifted toward higher wave numbers compared to the data collected at 340°. If this shift is associated with a built-in local strain, the strain can be estimated to be ~0.1 GPa [62, 63]. Higher resolution Raman measurements show that the major Raman peak at ~520 cm^{-1} is not only just slightly shifted but also broader compared to the spectrum collected from single crystal Si. In addition, we observe a second, much broader peak at ~504 cm^{-1}. The angular polarization dependence of the Raman signal at 504 cm^{-1} also deviates from the ⟨100⟩ oriented single-crystal Si reference, although this deviation is less significant compared to the Raman peak at ~520 cm^{-1}. The strong localization of strain observed in the Si matrix is consistent with our understanding of the nature of Stranski-Krastanov growth, where vertical self-ordering is produced by strain propagation through the separating Si layers [64].

5. PHOTOLUMINESCENCE PROPERTIES OF Si/SiGe THREE-DIMENSIONAL NANOSTRUCTURES AS A FUNCTION OF EXCITATION INTENSITY

It has been known for some time that the PL spectra in 3D Si/SiGe NSs, which is similar to that in III-V quantum

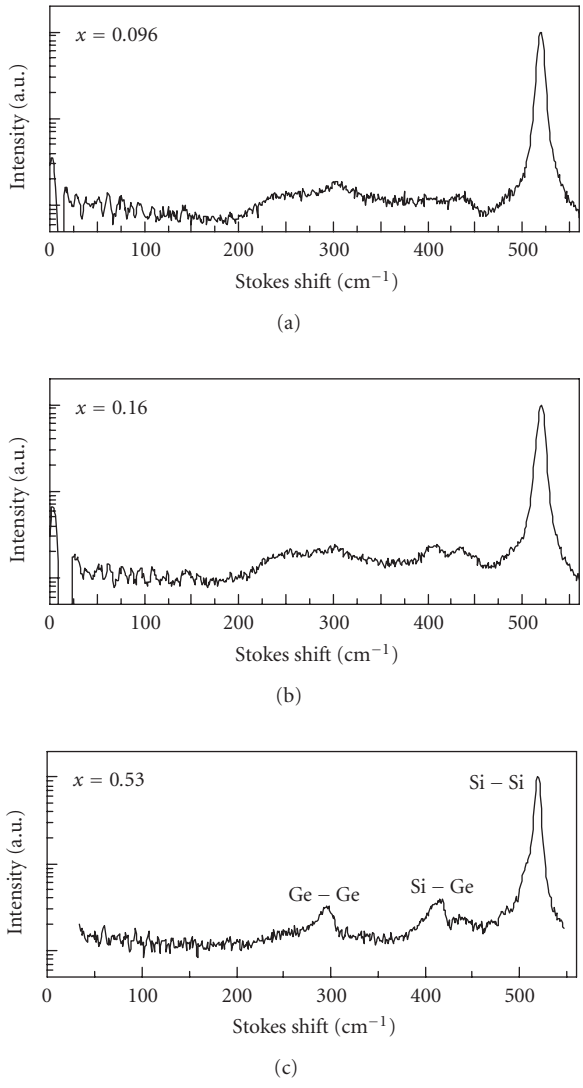

FIGURE 6: Raman spectra measured using 514 nm excitation in MBE grown $Si/Si_{1-x}Ge_x$ 3D NS samples with the indicated average Ge concentration x.

wells with type II energy band alignment [65], exhibit a blue shift as the excitation intensity increases [55, 66]. In our studies, this effect is found in both MBE and CVD grown samples. Figure 9(a) shows PL spectra in a CVD grown sample measured under excitation intensities varied from 0.1 to 100 W/cm^2. At the lowest excitation intensity used (0.1 W/cm^2), the PL peaks at ~0.8 eV. With increasing excitation intensity, a continuous almost parallel PL blue shift of 30–40 meV per decade of excitation intensity increase is observed. At an excitation intensity of 100 W/cm^2, the PL peak reaches ~0.92 eV. Under photoexcitation of 1–10 kW/cm^2, the low energy part of the PL spectrum does not shift further, while the high energy part continues shifting toward higher energy.

Figure 9(b) compares PL spectra measured with a fixed excitation intensity (~5 W/cm^2) for different temperatures in the range 8–210 K. These measurements clearly show that with increasing temperature, the PL peak associated with SiGe clusters at 0.85–0.9 eV shifts toward lower photon energies. This "red" PL spectral shift is, most likely, associated with the SiGe band gap decrease as the sample temperature increases. Thus, it is opposite to the "blue" PL spectrum shift observed with an excitation intensity increase, and thus this blue shift cannot simply be explained by sample heating due to the intense incident laser beam. There was some sample heating in the measurements, but it was not significant except at the higher laser powers. From the observed broadening of the PL spectral features associated with c–Si, the sample temperature is estimated to increase from 4 to 60 K under the highest excitation intensity used.

Despite the clear shift toward higher photon energy under increasing excitation intensity, the entire set of PL spectra recorded at photon energies <0.95 eV are well-fitted by two Gaussian peaks (shown in Figure 10(a) for the PL spectrum (1) obtained with 0.1 W/cm^2 excitation). Figure 10(b) summarizes the excitation intensity dependence of the energies of these two PL peak and their widths. For all PL spectra obtained at different excitation intensities, the two PL peaks at photon energies of ≤0.95 eV are found to be always separated by ~43 meV with a constant FWHM of ~78 and ~47 meV, respectively. These two PL peaks are attributed to the NP transition and TO phonon replica in the SiGe clusters, respectively, and the separation energy of ~43 meV is close to the energy of the TO Si–Ge phonon [30, 32–35, 47, 52–55]. The constant energy separation of the two PL peaks is additional evidence that, at the excitation intensities used, the observed PL blue shift is not due to thermal broadening caused by sample heating with the laser beam, and that the integrated PL intensities measured at different excitation intensities can be directly compared.

Figure 11 shows a modified (note the double logarithmic scale) Arrhenius plot of the normalized integrated PL intensity of a 3D Si/SiGe multilayer sample grown by CVD and measured at different excitation intensities. The normalized PL intensity temperature dependencies are fitted by a standard equation:

$$I_{PL}(T) = \frac{1}{[1 + C_1 \cdot \exp(-E_1/kT) + C_2 \cdot \exp(-E_2/kT)]}, \quad (1)$$

(see, e.g., [41]) with two thermal quenching activation energies E_1 and E_2. Here T is the temperature, k is Boltzmann's constant, and C_1 and C_2 are scaling coefficients. In all measurements for all samples, the PL thermal quenching activation energy $E_1 \approx 15$ meV and E_1 is independent of excitation intensity. In contrast, the activation energy E_2 depends significantly on the excitation intensity: the PL temperature dependence shows a step-like behavior, and E_2 increases dramatically from ~120 to 340 meV as the excitation intensity increases from 0.1 to 10 W/cm^2.

We start our discussion by noting that the observed excitation-independent PL thermal quenching activation

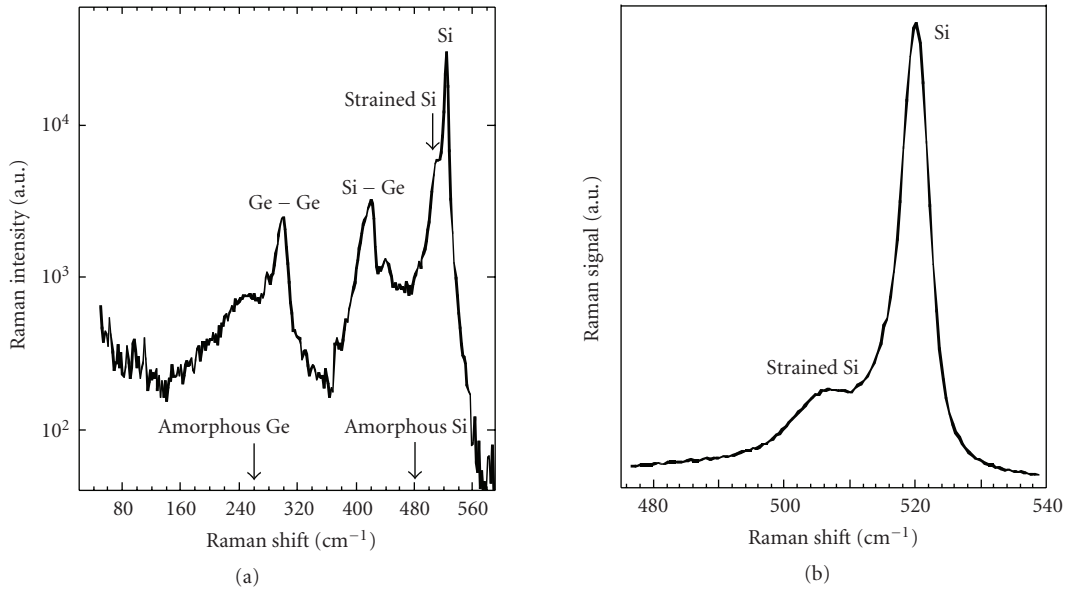

FIGURE 7: Raman spectra measured using 458 nm excitation in MBE grown $Si/Si_{1-x}Ge_x$ 3D NS samples with x approaching 50%. (a) A full-range spectrum comparing the major SiGe Raman modes with the positions of the Raman peaks seen in a-Si and a-Ge. (b) Raman spectrum on a linear intensity scale showing Si–Si vibrational modes including the vibration associated with strained Si at ~507 cm^{-1}.

energy of ~15 meV is close to the exciton binding energy in SiGe alloys and Si/SiGe superlattices [3, 14]. Thus, we conclude that one of the mechanisms of PL thermal quenching is the thermal dissociation of excitons. The activation energy of ~15 meV can therefore be associated with exciton localization in specific regions of the clusters associated with variations of the SiGe composition [1, 4]. Hence, the nonuniform SiGe cluster composition and, perhaps, variations in SiGe cluster size and shape could be responsible for the observed relatively broad PL spectra.

It has been proposed previously that 3D Si/SiGe nanostructures can be modeled using type-II energy band alignment, where, depending on the SiGe cluster size, valence band energy quantization is possible [41, 67]. Using the same model, we focus next on nonradiative carrier recombination and the different mechanisms of electron-hole separation. Electron transport in 3D Si/SiGe nanostructures is limited by a small (≤10–15 meV) conduction band energy barrier and SiGe compositional disorder [41]. Thus, the PL thermal quenching activation energy of ~15 meV could also be associated with electron diffusion in Si/SiGe 3D NSs.

In contrast, hole diffusion in 3D Si/SiGe multilayer NSs with a high Ge content is controlled by large (>100 meV) valence band energy barriers at Si/SiGe heterointerfaces [30, 40, 52, 68]. In this system, we consider two major mechanisms of hole transport: (i) hole tunneling and (ii) hole thermionic emission. Hole tunneling in 3D Si/SiGe NSs with thin (5–7 nm) Si separating layers and nearly perfect SiGe cluster vertical self-alignment could be very efficient. These nanostructures are usually grown by MBE and exhibit a PL thermal quenching activation energy of ~60 meV [41]. The same PL thermal quenching activation energy is found for the lowest excitation intensity in our CVD-grown samples with 7.5 nm thick Si separating layers. We suggest that in 3D Si/SiGe multilayer NSs with thin Si layers at low excitation intensity, the electron-hole separation and nonradiative carrier recombination are mainly controlled by hole tunneling between SiGe clusters. Due to significant variations in the SiGe cluster size, shape, and chemical composition, the process of hole tunneling could be assisted by phonon emission and/or absorption [69]. Therefore, the observed PL thermal quenching activation energy is close to the Si TO phonon energy [14]. In 3D Si/SiGe multilayer samples with 20 nm thick Si layers, where SiGe cluster vertical self-alignment is practically absent [42], the probability of hole tunneling is reduced, and hole thermionic emission over the Si/SiGe heterointerface barrier is playing a bigger role. Thus, in these samples the PL thermal quenching activation energy is expected to be greater, as has been found in our experiments (see Figure 11).

In this simple model, efficient hole tunneling between adjacent SiGe nanoclusters requires not only reasonably low and thin energy barriers but also a low carrier concentration (i.e., a large enough number of empty adjacent SiGe clusters). By increasing the photoexcitation intensity (i.e., the number of photogenerated carriers), hole tunneling can effectively be suppressed since fewer empty adjacent SiGe clusters can be found. At high excitation intensity, assuming (i) a negligible value of the conduction band offset compared to that in the valence band and (ii) a nearly pure Ge composition in the SiGe cluster core, the maximum anticipated PL thermal quenching activation energy should be $E_2 \leq E_g^{\mathrm{Si}} - E_g^{\mathrm{Ge}} \leq 400$ meV. This value sets the upper limit in the activation energy of PL intensity thermal quenching in 3D

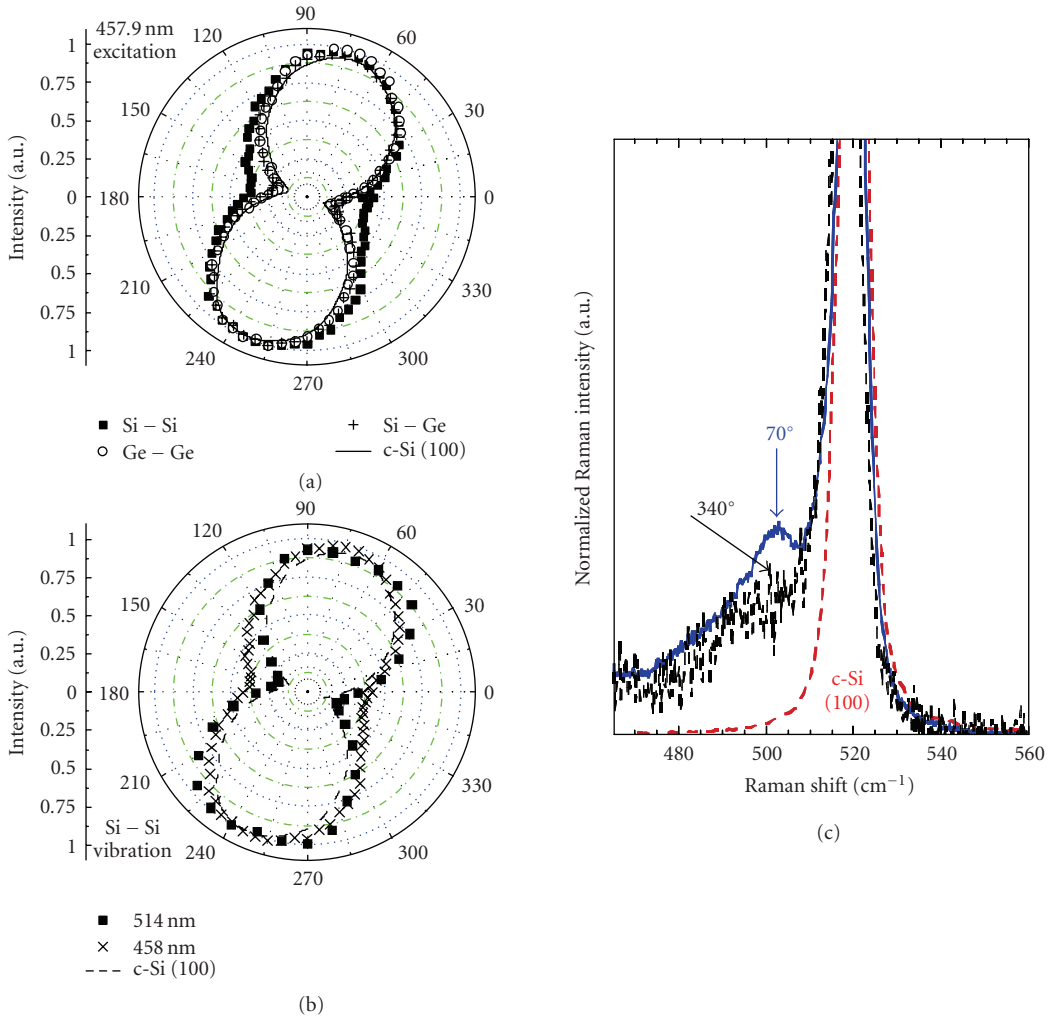

FIGURE 8: Polarization Raman polar diagrams in CVD grown SiGe 3D NS samples measured (a) for Si–Si, Si–Ge, and Ge–Ge vibrational modes using 458 nm excitation and (b) for the Si–Si vibrational mode using 458 and 514 nm excitation. The results obtained are compared with that of c–Si. (c) Raman spectra on a linear intensity scale in the vicinity of Si–Si vibrational modes in CVD-grown SiGe 3D NSs measured using two different polarization angles compared with that of c–Si.

SiGe multilayer NSs, and it is close to the activation energy of $E_2 \approx 340$ meV that has been found under the highest excitation intensity (see Figure 11).

6. PHOTOLUMINESCENCE DYNAMICS IN Si/SiGe THREE-DIMENSIONAL NANOSTRUCTURES

The PL dynamics, that is, the PL intensity decay under pulsed laser excitation, is an important technique for studying the carrier recombination mechanism. The PL decays discussed here were obtained using excitation by the second harmonic of a Q-switched YAG : Nd laser with photon energy $\hbar\omega = 2.33$ eV, pulse duration $\tau \approx 6$ nanoseconds, and repetition rate $\nu = 10$ Hz. The laser energy density on the sample was of the order of 1 mJ/cm^2. The PL signal in the 0.77–0.9 eV spectral region was recorded with an InGaAs photomultiplier tube (PMT) and stored in a digital LeCroy oscilloscope. The overall time resolution of the entire system was better than 20 nanoseconds.

Figure 12 shows the normalized PL decays collected from a CVD grown sample at 4 K. The initial PL decay is fast—close to the resolution of our detection system (<20 nanoseconds). The longer-lived PL shows a strong dependence on the detection photon energy, as summarized in Figure 13: the PL lifetime at photon energies below 0.8 eV is found to be ~20 microseconds, and it drastically decreases to ~200 nanoseconds for the PL component measured at 0.89 eV.

Such a dramatic (100 times) decrease in the PL lifetime provides key information about the carrier recombination mechanism and this will be discussed later.

7. ELECTROLUMINESCENCE IN Si/SiGe THREE-DIMENSIONAL NANOSTRUCTURES

Electroluminescence (EL) in 3D Si/SiGe NSs was found almost simultaneously with the first investigations of the PL [22, 30]. In many of the Si-based nanostructures with

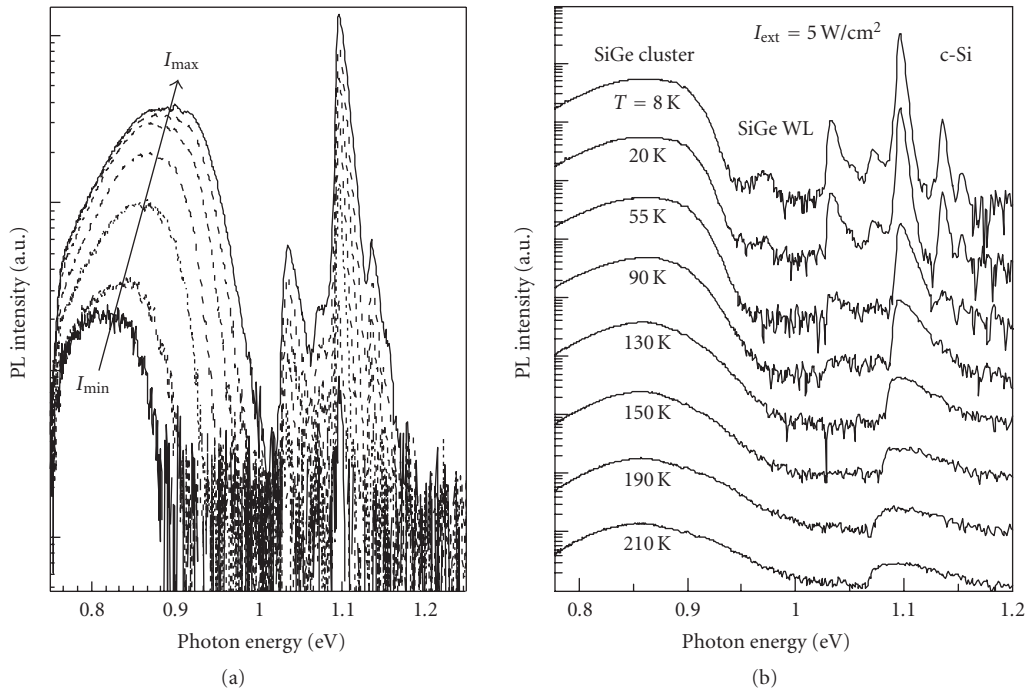

FIGURE 9: PL spectra in CVD grown Si/SiGe 3D NSs (a) measured at $T = 4$ K under different excitation intensities from I_{min} (0.1 W/cm^2) to I_{max} (100 W/cm^2) and (b) under a fixed excitation intensity of 5 W/cm^2 at the indicated temperatures (the PL spectra have been shifted vertically for clarity).

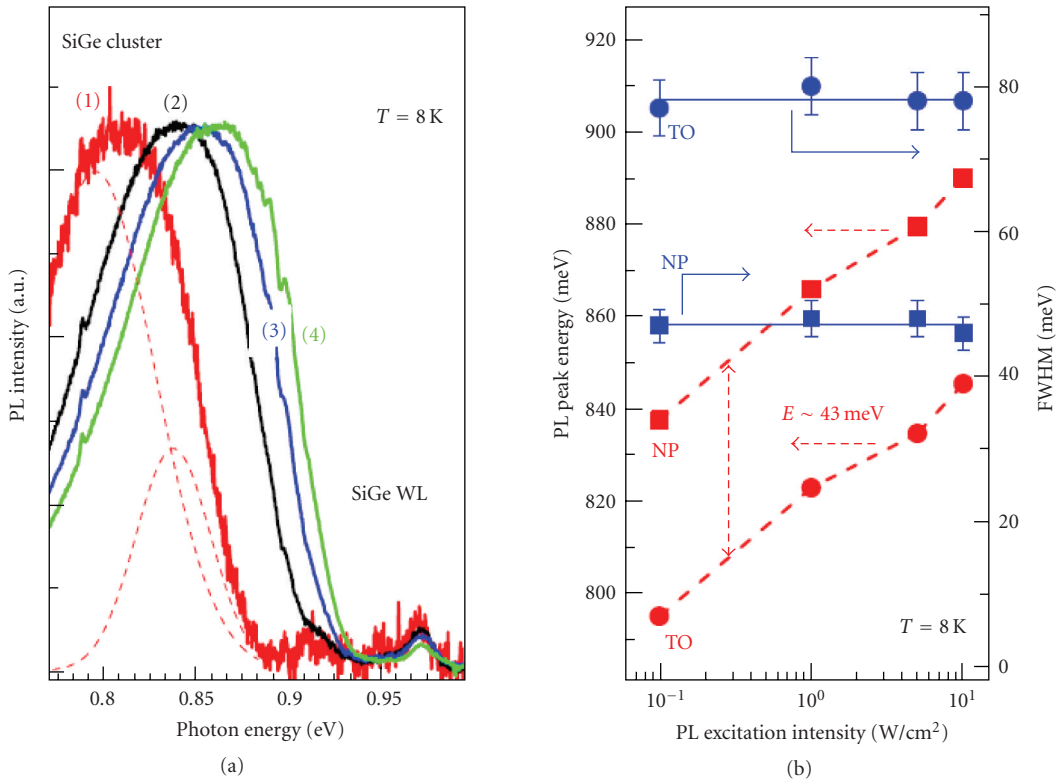

FIGURE 10: (a) Normalized PL spectra in CVD grown Si/SiGe 3D NSs showing the PL spectral shift to higher photon energy under increasing excitation intensity. Each spectrum can be fitted with two (NP and TO) Gaussian spectral bands, as shown, for example, by the dashed lines under trace (1). (b) Summary of PL spectra changes as a function of excitation intensity.

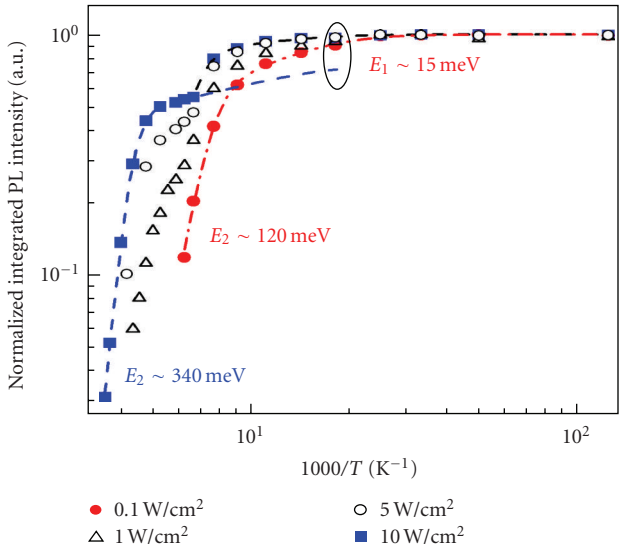

FIGURE 11: Typical integrated PL intensity for CVD grown samples as a function of the reciprocal temperature measured under different excitation intensities, as indicated. The activation energies obtained from fits (shown by the different lines) to the data (shown by the different points) are also given.

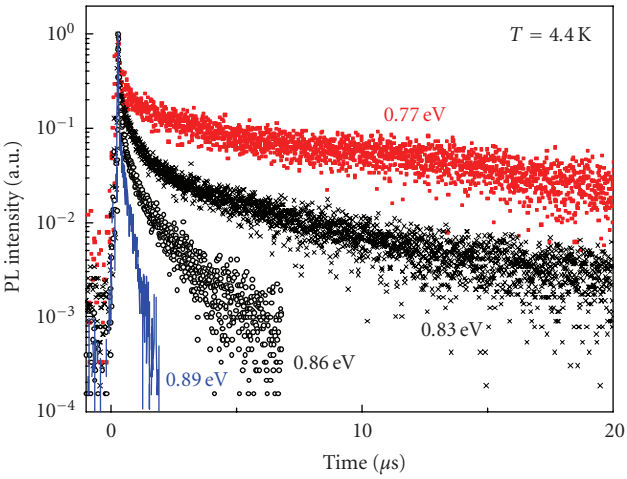

FIGURE 12: Typical low temperature ($T = 4$ K) PL dynamics for CVD grown samples measured at the indicated photon energies using a short (~6 nanoseconds) excitation pulse.

promising PL properties (e.g., Si nanocrystals embedded in silicon oxide, Er+ in silicon-rich silicon oxide, etc.), EL is difficult to obtain due to poor carrier transport [11, 15, 20]. In contrast, vertical carrier transport in Si/SiGe multilayers and 3D Si/SiGe NSs is very efficient, and a simple device where Si/SiGe multilayers are embedded into a p-i-n diode or a similar structure can easily be fabricated [22, 33]. Figure 14 proves this statement by showing EL spectra for a CVD grown sample measured under a relatively low value of forward bias of 3–6 V applied to a Schottky-barrier type structure. The measured EL spectrum is broad

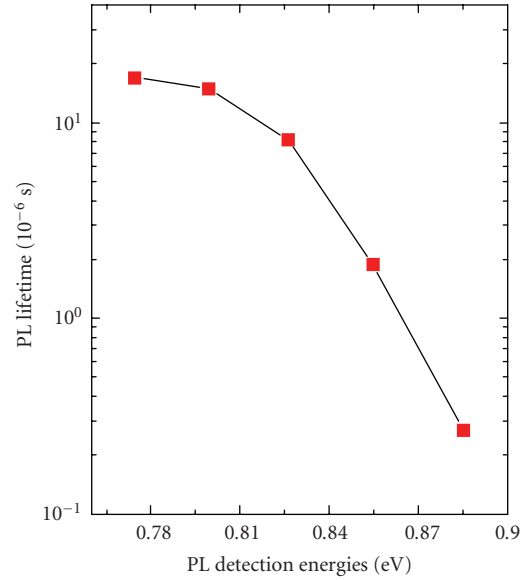

FIGURE 13: Summary of PL lifetimes for CVD grown samples at different photon energies.

with an asymmetric spectral shape, which, similar to the PL spectra, can be well fitted by two Gaussian bands separated by ~45 meV. This separation energy is close to an SiGe characteristic phonon energy, proving that the EL mechanism is nearly identical to the PL one, that is, it is due to radiative electron-hole recombination in 3D Si/SiGe layered NSs. On increasing the applied voltage, we observe (similar to that in PL spectra under increasing photoexcitation intensity) a noticeable EL spectral shift toward greater photon energies, that is, a "blue shift" (see Figure 14). The integrated EL intensity is nearly a linear function of the applied voltage (Figure 15). The EL intensity as a function of temperature is also similar to that found in PL, and the EL thermal quenching activation energy is ~130 meV (Figure 16(b)). Interestingly, in the same sample, the device current as a function of temperature depicts nearly an exact anticorrelation with the EL intensity and exhibits an activation energy of ~140 meV (Figure 16(a)).

8. MECHANISM OF CARRIER RECOMBINATION AND LIGHT EMISSION IN Si/SiGe THREE-DIMENSIONAL NANOSTRUCTURES

In our discussion on carrier recombination in 3D Si/SiGe NSs, we focus on MBE and CVD grown samples with an average Ge atomic composition close to 50%. Several experimental results, including the PL spectral distribution extending well below the band gap of pure Ge [33–35] and the extremely long carrier radiative lifetime of ~10 milliseconds [41], as well as the ~30 meV per decade PL spectral shift toward higher photon energies as the excitation intensity increases [70], point out strong similarities between the PL in 3D Si/SiGe NSs and the PL in III-V quantum

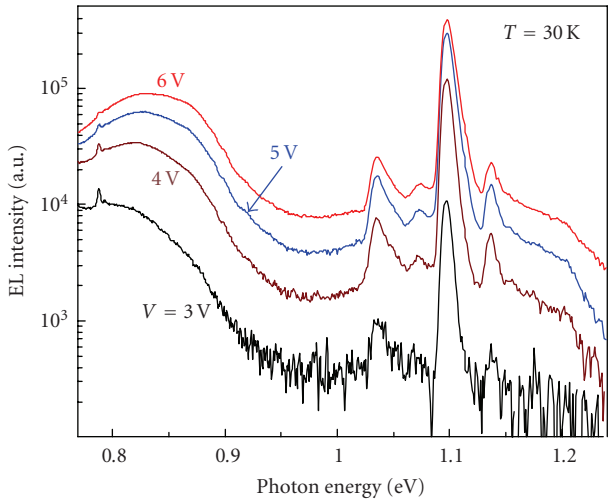

FIGURE 14: EL spectra of a CVD grown sample at $T = 30$ K detected using pulsed electrical excitation at the indicated voltage amplitudes.

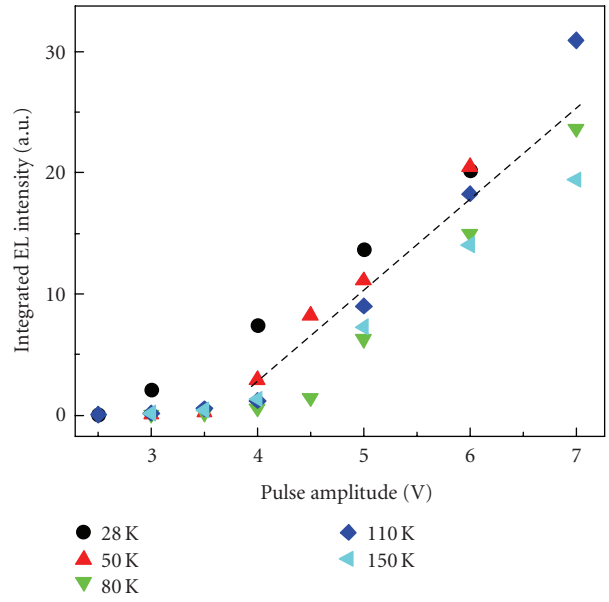

FIGURE 15: Integrated EL intensity over the 0.75–0.95 eV spectral region of a CVD grown sample as a function of the pulsed voltage amplitude measured at the indicated temperatures. The dashed straight line is a guide to the eye.

wells with type-II energy band alignment [65, 66]. Generally, a type-II energy band alignment at the heterointerface is a strong disadvantage for light emitting devices due to a weak overlap between spatially separated electron and hole wave functions. In reality, however, the critical limitation in the efficiency of light-emitting structures is rather the presence of competing nonradiative recombination channels for excess electrons and holes. The most important nonradiative mechanism is carrier recombination via defects, especially heterointerface structural defects such as propagating dislocations and dislocation complexes. The 3D Si/SiGe NSs investigated here, grown by both MBE and CVD processes, show an almost undetectable density of dislocations [24, 30]. Thus, in these well grown 3D Si/SiGe NSs, we can neglect nonradiative carrier recombination via structural defects, and this explains the experimentally observed high quantum efficiency of PL with photon energy <0.9 eV, which is associated with SiGe clusters, at low excitation intensities.

It has been suggested that SiGe Stranski-Krastanov (S-K) clusters with a small (3–5 nm) height and greater than 10 : 1 base-to-height aspect ratio can be modeled as nanostructures with a type-II energy band alignment and possibly with SiGe cluster valence-band energy quantization in the direction of growth [39–41, 53]. Strained Si and Si-rich SiGe alloy regions near the base of the clusters (also called SiGe wetting layers) also need to be considered [42]. In our samples, the PL associated with the c–Si separating layers exhibits unusual doublet-like structures (Figure 3), most likely due to the built-in strain. Including the effect of strain, the observed PL bands at 0.916 and 0.972 eV indicate a composition of the $Si_{1-x}Ge_x$ transition region, which is presumably located near the bottom of the Ge/Si pyramid-like clusters, to be close to $x \approx 0.2$ [30]. This conclusion is supported by recent direct analytical TEM measurements [42–45].

It has also been proposed that the broad PL band with a peak energy of ~0.8–0.9 eV is due to the recombination of carriers localized in the Ge-richest areas of the clusters, which is close to the center of "pancake" shaped SiGe clusters [43, 44]. We suggest that at the lowest excitation intensity, the PL arises from electron-hole recombination between holes localized in the Ge-richest regions of the cluster and electrons localized in the strained SiGe alloy region near the cluster base. This immediately explains the extension of the observed PL spectrum below the pure Ge band gap energy.

On increasing the excitation intensity, we find that the high-photon-energy edge of the Ge-rich cluster PL eventually overlaps with PL originating from the $Si_{1-x}Ge_x$ alloy region with $x \approx 0.2$. Theoretical calculations predict that strained $Si/Si_{1-x}Ge_x$ two-dimensional NSs with $x \approx 0.2$ might have type-I energy band alignment [36]. The SiGe clusters embedded in the Si matrix can induce local strain mainly in the SiGe alloy region near the bottom of the Ge cluster. We attribute the observed decrease of the PL lifetime (presumably radiative lifetime) detected between 0.8 and 0.9 eV in our experiments to an increasing contribution from fast radiative transitions involving locally strained SiGe regions of lower Ge concetration at the bottom of SiGe clusters.

Figure 17 summarizes in schematic form the proposed model of radiative carrier recombination in 3D Si/SiGe NSs. It illustrates that, at low excitation intensity, the observed PL at photon energies $\hbar\omega < 0.8$ eV is due to slow recombination between electrons localized within a strained Si-rich $Si_{1-x}Ge_x$ region with $x \approx 0.2$ and holes occupying the lowest energy states in the Ge-rich cluster core. An increase in the excitation power in PL experiments, as well as the current density in EL experiments, usually leads to changes in the emission spectra; for example, the PL and EL peaks blue shift, that is, they shift toward shorter wavelength (see Figures 9, 10, and 14). At the same time, the PL intensity as a function of excitation

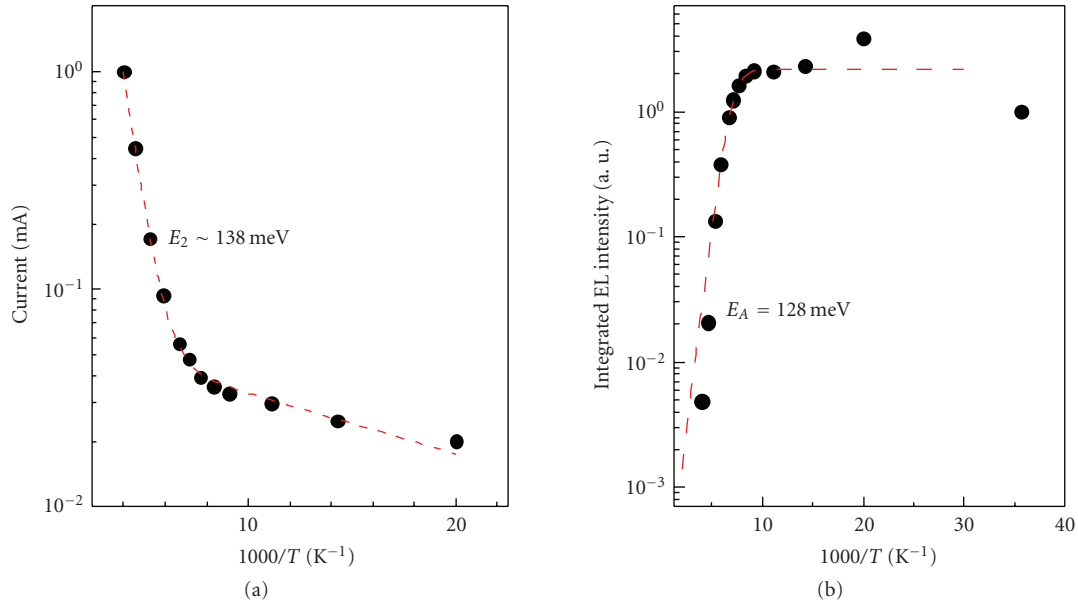

FIGURE 16: (a) Current and (b) EL intensity as a function of the reciprocal temperature for a CVD grown sample. The activation energies obtained from fits to the data (dashed lines) are also shown.

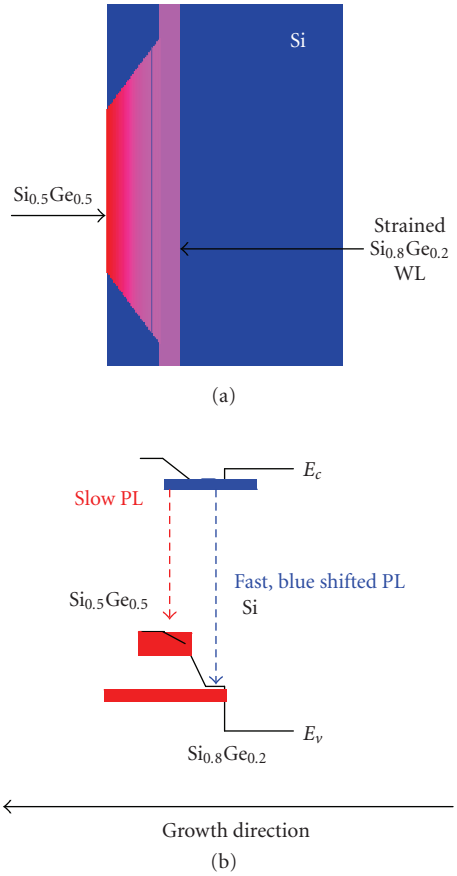

FIGURE 17: (a) Schematic representation of the atomic structure of an SiGe nanocluster on a wetting layer with a core Ge concentration close to 50% embedded into an Si matrix and (b) the corresponding energy band diagram with two possible radiative transitions indicated.

intensity in MBE grown 3D Si/SiGe NSs displays a sublinear dependence on a logarithmic scale (Figure 4). It has been pointed out that possible transformations of hole energy spectra due to quantization and/or strain might dramatically increase the rate of nonradiative Auger recombination, by more than 100 times compared to that in bulk Si and Ge [71]. However, in a quantum well with smoothed (e.g., diffused) heterointerfaces, Auger processes are expected to be less efficient [35, 41]. We find strong evidence that in CVD grown 3D Si/SiGe NSs the reduction of the Auger rate, most likely due to diffused Si/SiGe interfaces, does take place. Thus, on increasing the pumping power in PL experiments on CVD grown samples, we observe a relatively small deviation from a linear function in the PL intensity dependence on excitation (see Figure 9). In addition, we find that the previously mentioned PL spectral blue shift, with the PL peak shifting from a photon energy of 0.78 to 0.88 eV, correlates with a strong (~100 times) decrease in the carrier radiative lifetime (Figures 9, 10, 12, and 13). The hole energy barrier between the strained $Si_{0.8}Ge_{0.2}$ transition region and Si is ≥ 200 meV, in good agreement with a larger value of the observed PL thermal quenching activation energy, while the smaller value of 15 meV is closer to the exciton binding energy in SiGe alloys, as has been previously discussed [35, 41, 72].

Figure 17 also proposes an energy band diagram, which takes into account the previously described complex compositional structure of 3D Si/SiGe heterointerfaces. It shows a modified type-II energy band alignment at the SiGe cluster core with a compositional transition toward the Si/SiGe heterointerface and a nearly type-I alignment at the cluster base, mainly due to the strain in the SiGe wetting layer. A continuous change in the Ge atomic concentration is reflected by a gradually increasing energy band gap from the cluster center toward the SiGe wetting layer, where the Ge

atomic concentration is estimated to be ∼20%. In this band diagram, two types of radiative transitions are shown (Figure 17(b)). First, there is a slow recombination between electrons localized mainly in the SiGe wetting layer and holes localized within SiGe clusters, mostly near the SiGe cluster core. Second, a faster and more efficient radiative recombination is achieved between electrons and holes leaking from the SiGe cluster core toward the cluster base and SiGe wetting layer. This latter recombination mechanism, which becomes dominant under a high photoexcitation intensity when the "slow" recombination channel for spatially separated electrons and holes is saturated, has been called a "dynamic type-I" energy band alignment [41, 70]. It explains very well both the PL spectral blue shift under increasing excitation intensity and the dramatic (∼100 times) decrease in carrier radiative lifetime measured at photon energies from 0.77 to 0.89 eV. This explanation is also consistent with the previously discussed PL intensity temperature dependence, which shows a different PL thermal quenching activation energy at different excitation intensities (see also [72]).

9. CONCLUSION

In conclusion, we present comprehensive experimental studies on Raman scattering and light-emitting (PL and EL) properties of 3D Si/SiGe NSs. We show that these nanostructures emit light at the technologically important 1.3–1.6 μm wavelength region. The highest PL and EL quantum efficiency is found in SiGe clusters with an ∼50% Ge composition near the cluster core. The highest luminescence quantum efficiency is observed at low excitation intensity. However, the PL quantum efficiency decreases as the excitation intensity increases, most likely due to competition with a faster nonradiative Auger recombination. Using time resolved PL measurements, we found that the suspected type-II energy band alignment at the Si/SiGe cluster heterointerface is responsible for the observed long carrier radiative lifetime (10^{-4}–10^{-3} second). We also found that within the broad PL band, the part of the PL spectra associated with higher photon energies exhibits an ∼100 times faster radiative transition, which is explained by a proposed "dynamic type-I" energy band alignment, for example, radiative recombination between holes occupying excited states in SiGe clusters and electrons mostly localized close to the $Si_{1-x}Ge_x$ wetting layer with $x \approx 0.2$. These experimental observations suggest that a commercially useful SiGe light-emitting device can be fabricated and integrated into the traditional CMOS environment.

ACKNOWLEDGMENTS

The authors would like to thank Xiaohua Wu for the TEM results from an MBE grown sample shown in Figure 1. L. Tsybeskov acknowledges partial support for this project provided by the US National Science Foundation, Intel Corp., Semiconductor Research Corporation, and Foundation at NJIT.

REFERENCES

[1] N. Savage, "Linking with light," *IEEE Spectrum*, vol. 39, no. 8, pp. 32–36, 2002.
[2] B. Mukherjee, "WDM optical communication networks: progress and challenges," *IEEE Journal on Selected Areas in Communications*, vol. 18, no. 10, pp. 1810–1824, 2000.
[3] D. V. Plant and A. G. Kirk, "Optical interconnects at the chip and board level: challenges and solutions," *Proceedings of the IEEE*, vol. 88, no. 6, pp. 806–818, 2000.
[4] D. A. B. Miller, "Rationale and challenges for optical interconnects to electronic chips," *Proceedings of the IEEE*, vol. 88, no. 6, pp. 728–749, 2000.
[5] D. A. B. Miller, "Optical interconnects to silicon," *IEEE Journal on Selected Topics in Quantum Electronics*, vol. 6, no. 6, pp. 1312–1317, 2000.
[6] H. Wada and T. Kamijoh, "Room-temperature CW operation of InGaAsP lasers on Si fabricated by wafer bonding," *IEEE Photonics Technology Letters*, vol. 8, no. 2, pp. 173–175, 1996.
[7] M. Razeghi, M. Defour, R. Blondeau, et al., "First cw operation of a $Ga_{0.25}In_{0.75}As_{0.5}P_{0.5}$-InP laser on a silicon substrate," *Applied Physics Letters*, vol. 53, no. 24, pp. 2389–2390, 1988.
[8] H. Park, A. W. Fang, S. Kodama, and J. E. Bowers, "Hybrid silicon evanescent laser fabricated with a silicon waveguide and III-V offset quantum wells," *Optics Express*, vol. 13, no. 23, pp. 9460–9464, 2005.
[9] A. W. Fang, H. Park, O. Cohen, R. Jones, M. J. Paniccia, and J. E. Bowers, "Electrically pumped hybrid AlGaInAs-silicon evanescent laser," *Optics Express*, vol. 14, no. 20, pp. 9203–9210, 2006.
[10] L. Pavesi and D. J. Lockwood, *Silicon Photonics*, Springer, Berlin, Germany, 2004.
[11] Y. Kanemitsu, "Light emission from porous silicon and related materials," *Physics Report*, vol. 263, no. 1, pp. 1–91, 1995.
[12] K. D. Hirschman, L. Tsybeskov, S. P. Duttagupta, and P. M. Fauchet, "Silicon-based visible light-emitting devices integrated into microelectronic circuits," *Nature*, vol. 384, no. 6607, pp. 338–341, 1996.
[13] A. G. Cullis, L. T. Canham, and P. D. J. Calcott, "The structural and luminescence properties of porous silicon," *Journal of Applied Physics*, vol. 82, no. 3, pp. 909–965, 1997.
[14] Z. H. Lu, D. J. Lockwood, and J.-M. Baribeau, "Quantum confinement and light emission in SiO_2/Si superlattices," *Nature*, vol. 378, no. 6553, pp. 258–260, 1995.
[15] L. Tsybeskov and D. J. Lockwood, "Nanocrystalline silicon-silicon dioxide superlattices: structural and optical properties," in *Semiconductor Nanocrystals: From Basic Principles to Applications*, A. L. Efros, D. J. Lockwood, and L. Tsybeskov, Eds., pp. 209–229, Kluwer Academics/Plenum Publishers, New York, NY, USA, 2003.
[16] G. F. Grom, D. J. Lockwood, J. P. McCaffrey, et al., "Ordering and self-organization in nanocrystalline silicon," *Nature*, vol. 407, no. 6802, pp. 358–361, 2000.
[17] L. Tsybeskov, K. D. Hirschman, S. P. Duttagupta, et al., "Nanocrystalline-silicon superlattice produced by controlled recrystallization," *Applied Physics Letters*, vol. 72, no. 1, pp. 43–45, 1998.
[18] L. Pavesi, L. Dal Negro, C. Mazzoleni, G. Franzò, and F. Priolo, "Optical gain in silicon nanocrystals," *Nature*, vol. 408, no. 6811, pp. 440–444, 2000.
[19] S. Schuppler, S. L. Friedman, M. A. Marcus, et al., "Size, shape, and composition of luminescent species in oxidized Si nanocrystals and H-passivated porous Si," *Physical Review B*, vol. 52, no. 7, pp. 4910–4925, 1995.

[20] S. Coffa, G. Franzò, and F. Priolo, "High efficiency and fast modulation of Er-doped light emitting Si diodes," *Applied Physics Letters*, vol. 69, no. 14, pp. 2077–2079, 1996.

[21] S. Fukatsu, N. Usami, Y. Shiraki, A. Nishida, and K. Nakagawa, "High-temperature operation of strained $Si_{0.65}Ge_{0.35}$/Si(111) *p*-type multiple-quantum-well light-emitting diode grown by solid source Si molecular-beam epitaxy," *Applied Physics Letters*, vol. 63, no. 7, pp. 967–969, 1993.

[22] L. Vescan and T. Stoica, "Room-temperature SiGe light-emitting diodes," *Journal of Luminescence*, vol. 80, no. 1–4, pp. 485–489, 1998.

[23] D. Leong, M. Harry, K. J. Reeson, and K. P. Homewood, "A silicon/iron-disllicide light-emitting diode operating at a wavelength of 1.5 μm," *Nature*, vol. 387, no. 6634, pp. 686–688, 1997.

[24] D. J. Eaglesham and M. Cerullo, "Dislocation-free Stranski-Krastanow growth of Ge on Si(100)," *Physical Review Letters*, vol. 64, no. 16, pp. 1943–1946, 1990.

[25] Y.-W. Mo, D. E. Savage, B. S. Swartzentruber, and M. G. Lagally, "Kinetic pathway in Stranski-Krastanov growth of Ge on Si(001)," *Physical Review Letters*, vol. 65, no. 8, pp. 1020–1023, 1990.

[26] D. E. Savage, F. Liu, V. Zielasek, and M. G. Lagaly, "Fundamental mechanisms of film growth," in *Germanium Silicon: Growth and Materials*, R. Hull and J. C. Bean, Eds., vol. 56 of *Semiconductor and Semimetals*, pp. 49–96, Academic Press, New York, NY, USA, 1999.

[27] B. Voigtländer and A. Zinner, "Simultaneous molecular beam epitaxy growth and scanning tunneling microscopy imaging during Ge/Si epitaxy," *Applied Physics Letters*, vol. 63, no. 22, pp. 3055–3057, 1993.

[28] J. A. Flora, E. Chason, L. B. Freund, R. D. Twesten, R. Q. Hwang, and G. A. Lucadamo, "Evolution of coherent islands in $Si_{1-x}Ge_x$/Si(001)," *Physical Review B*, vol. 59, no. 3, pp. 1990–1998, 1999.

[29] D. E. Jesson, S. J. Pennycook, J. Z. Tischler, J. D. Budai, J.-M. Baribeau, and D. C. Houghton, "Interplay between evolving surface morphology, atomic-scale growth modes, and ordering during Si_xGe_{1-x} epitaxy," *Physical Review Letters*, vol. 70, no. 15, pp. 2293–2296, 1993.

[30] Y. Shiraki and A. Sakai, "Fabrication technology of SiGe hetero-structures and their properties," *Surface Science Reports*, vol. 59, no. 7-8, pp. 153–207, 2005.

[31] T. I. Kamins, E. C. Carr, R. S. Williams, and S. J. Rosner, "Deposition of three-dimensional Ge islands on Si(001) by chemical vapor deposition at atmospheric and reduced pressures," *Journal of Applied Physics*, vol. 81, no. 1, pp. 211–219, 1997.

[32] P. Schittenhelm, M. Gail, J. Brunner, J. F. Nützel, and G. Abstreiter, "Photoluminescence study of the crossover from two-dimensional to three-dimensional growth for Ge on Si(100)," *Applied Physics Letters*, vol. 67, no. 9, pp. 1292–1294, 1995.

[33] R. Apetz, L. Vescan, A. Hartmann, C. Dieker, and H. Lüth, "Photoluminescence and electroluminescence of SiGe dots fabricated by island growth," *Applied Physics Letters*, vol. 66, no. 4, pp. 445–447, 1995.

[34] O. G. Schmidt, C. Lange, and K. Eberl, "Photoluminescence study of the initial stages of island formation for Ge pyramids/domes and hut clusters on Si(001)," *Applied Physics Letters*, vol. 75, no. 13, pp. 1905–1907, 1999.

[35] B. V. Kamenev, L. Tsybeskov, J.-M. Baribeau, and D. J. Lockwood, "Photoluminescence and Raman scattering in three-dimensional Si/$Si_{1-x}Ge_x$ nanostructures," *Applied Physics Letters*, vol. 84, no. 8, pp. 1293–1295, 2004.

[36] C. G. Van de Walle and R. M. Martin, "Theoretical calculations of heterojunction discontinuities in the Si/Ge system," *Physical Review B*, vol. 34, no. 8, pp. 5621–5634, 1986.

[37] D. C. Houghton, G. C. Aers, S.-R. Eric Yang, E. Wang, and N. L. Rowell, "Type I band alignment in $Si_{1-x}Ge_x$/Si(001) quantum wells: photoluminescence under applied [110] and [100] uniaxial stress," *Physical Review Letters*, vol. 75, no. 5, pp. 866–869, 1995.

[38] M. L. W. Thewalt, D. A. Harrison, C. F. Reinhart, J. A. Wolk, and H. Lafontaine, "Type II band alignment in $Si_{1-x}Ge_x$/Si(001) quantum wells: the ubiquitous type I luminescence results from band bending," *Physical Review Letters*, vol. 79, no. 2, pp. 269–272, 1997.

[39] P. Schittenhelm, C. Engel, F. Findeis, et al., "Self-assembled Ge dots: growth, characterization, ordering, and applications," *Journal of Vacuum Science & Technology B*, vol. 16, no. 3, pp. 1575–1581, 1998.

[40] M. El Kurdi, S. Sauvage, G. Fishman, and P. Boucaud, "Band-edge alignment of SiGe Si quantum wells and SiGe Si self-assembled islands," *Physical Review B*, vol. 73, no. 19, Article ID 195327, 9 pages, 2006.

[41] B. V. Kamenev, L. Tsybeskov, J.-M. Baribeau, and D. J. Lockwood, "Coexistence of fast and slow luminescence in three-dimensional Si/$Si_{1-x}Ge_x$ nanostructures," *Physical Review B*, vol. 72, no. 19, Article ID 193306, 4 pages, 2005.

[42] J.-M. Baribeau, N. L. Rowell, and D. J. Lockwood, "Advances in the growth and characterization of Ge quantum dots and islands," *Journal of Materials Research*, vol. 20, no. 12, pp. 3278–3293, 2005.

[43] J.-M. Baribeau, X. Wu, and D. J. Lockwood, "Probing the composition of Ge dots and Si/$Si_{1-x}Ge_x$ island superlattices," *Journal of Vacuum Science & Technology A*, vol. 24, no. 3, pp. 663–667, 2006.

[44] J.-M. Baribeau, X. Wu, M.-J. Picard, and D. J. Lockwood, "Characterization of coherent $Si_{1-x}Ge_x$ island superlattices on (100) Si," in *Proceedings of the Materials Research Society Fall Meeting, Group IV Semiconductor Nanostructures*, L. Tsybeskov, D. J. Lockwood, C. Delerue, M. Ichikawa, and A. W. van Buuren, Eds., vol. 958, pp. 119–124, Boston, Mass, USA, November-December 2006.

[45] D. J. Lockwood, X. Wu, and J.-M. Baribeau, "Compositional redistribution in coherent $Si_{1-x}Ge_x$ islands on Si(100)," *IEEE Transactions on Nanotechnology*, vol. 6, no. 2, pp. 245–249, 2007.

[46] B. V. Kamenev, H. Grebel, L. Tsybeskov, et al., "Polarized Raman scattering and localized embedded strain in self-organized Si/Ge nanostructures," *Applied Physics Letters*, vol. 83, no. 24, pp. 5035–5037, 2003.

[47] L. P. Tilly, P. M. Mooney, J. O. Chu, and F. K. LeGoues, "Near band-edge photoluminescence in relaxed $Si_{1-x}Ge_x$ layers," *Applied Physics Letters*, vol. 67, no. 17, pp. 2488–2490, 1995.

[48] A. Zrenner, B. Fröhlich, J. Brunner, and G. Abstreiter, "Time-resolved photoluminescence of pseudomorphic SiGe quantum wells," *Physical Review B*, vol. 52, no. 23, pp. 16608–16611, 1995.

[49] M. Chen, D. L. Smith, and T. C. McGill, "Low-temperature photoluminescence spectra of doped Ge," *Physical Review B*, vol. 15, no. 10, pp. 4983–4996, 1977.

[50] J.-M. Baribeau, X. Wu, N. L. Rowell, and D. J. Lockwood, "Ge dots and nanostructures grown epitaxially on Si," *Journal of Physics Condensed Matter*, vol. 18, no. 8, pp. R139–R174, 2006.

[51] S. Bozzo, J.-L. Lazzari, G. Bremond, and J. Derrien, "Temperature and excitation power dependencies of the photoluminescence of planar and vertically self-organized $Si_{0.70}Ge_{0.30}$/Si strained superlattices," *Thin Solid Films*, vol. 380, no. 1-2, pp. 130–133, 2000.

[52] O. G. Schmidt and K. Eberl, "Multiple layers of self-assembled Ge/Si islands: photoluminescence, strain fields, material interdiffusion, and island formation," *Physical Review B*, vol. 61, no. 20, pp. 13721–13729, 2000.

[53] K. Brunner, "Si/Ge nanostructures," *Reports on Progress in Physics*, vol. 65, no. 1, pp. 27–72, 2002.

[54] J. C. Sturm, H. Manoharan, L. C. Lenchyshyn, et al., "Well-resolved band-edge photoluminescence of excitons confined in strained $Si_{1-x}Ge_x$ quantum wells," *Physical Review Letters*, vol. 66, no. 10, pp. 1362–1365, 1991.

[55] L. C. Lenchyshyn, M. L. W. Thewalt, J. C. Sturm, et al., "High quantum efficiency photoluminescence from localized excitons in $Si_{1-x}Ge_x$," *Applied Physics Letters*, vol. 60, no. 25, pp. 3174–3176, 1992.

[56] H. Sunamura, Y. Shiraki, and S. Fukatsu, "Growth mode transition and photoluminescence properties of $Si_{1-x}Ge_x$/Si quantum well structures with high Ge composition," *Applied Physics Letters*, vol. 66, no. 8, pp. 953–955, 1995.

[57] J. Weber and M. I. Alonso, "Near-band-gap photoluminescence of Si-Ge alloys," *Physical Review B*, vol. 40, no. 8, pp. 5683–5693, 1989.

[58] P. A. Temple and C. E. Hathaway, "Multiphonon Raman spectrum of silicon," *Physical Review B*, vol. 7, no. 8, pp. 3685–3697, 1973.

[59] M. I. Alonso and K. Winer, "Raman spectra of c-$Si_{1-x}Ge_x$ alloys," *Physical Review B*, vol. 39, no. 14, pp. 10056–10062, 1989.

[60] J. E. Smith Jr., M. H. Brodsky, B. L. Crowder, M. I. Nathan, and A. Pinczuk, "Raman spectra of amorphous Si and related tetrahedrally bonded semiconductors," *Physical Review Letters*, vol. 26, no. 11, pp. 642–646, 1971.

[61] W. L. Henstrom, C.-P. Liu, J. M. Gibson, T. I. Kamins, and R. S. Williams, "Dome-to-pyramid shape transition in Ge/Si islands due to strain relaxation by interdiffusion," *Applied Physics Letters*, vol. 77, no. 11, pp. 1623–1625, 2000.

[62] F. Cerdeira, C. J. Buchenauer, F. H. Pollak, and M. Cardona, "Stress-induced shifts of first-order Raman frequencies of diamond- and zinc-blende-type semiconductors," *Physical Review B*, vol. 5, no. 2, pp. 580–593, 1972.

[63] S. C. Jain, B. Dietrich, H. Richter, A. Atkinson, and A. H. Harker, "Stresses in strained GeSi stripes: calculation and determination from Raman measurements," *Physical Review B*, vol. 52, no. 9, pp. 6247–6253, 1995.

[64] J. Tersoff, C. Teichert, and M. G. Lagally, "Self-organization in growth of quantum dot superlattices," *Physical Review Letters*, vol. 76, no. 10, pp. 1675–1678, 1996.

[65] J. Hu, X. G. Xu, J. A. H. Stotz, et al., "Type II photoluminescence and conduction band offsets of GaAsSb/InGaAs and GaAsSb/InP heterostructures grown by metalorganic vapor phase epitaxy," *Applied Physics Letters*, vol. 73, no. 19, pp. 2799–2801, 1998.

[66] T. Baier, U. Mantz, K. Thonke, R. Sauer, F. Schäffler, and H.-J. Herzog, "Type-II band alignment in Si/$Si_{1-x}Ge_x$ quantum wells from photoluminescence line shifts due to optically induced band-bending effects: experiment and theory," *Physical Review B*, vol. 50, no. 20, pp. 15191–15196, 1994.

[67] J. Wan, G. L. Jin, Z. M. Jiang, Y. H. Luo, J. L. Liu, and K. L. Wang, "Band alignments and photon-induced carrier transfer from wetting layers to Ge islands grown on Si(001)," *Applied Physics Letters*, vol. 78, no. 12, pp. 1763–1765, 2001.

[68] P. A. Cain, H. Ahmed, D. A. Williams, and J. M. Bonar, "Hole transport through single and double SiGe quantum dots," *Applied Physics Letters*, vol. 77, no. 21, pp. 3415–3417, 2000.

[69] H. Qin, A. W. Holleitner, K. Eberl, and R. H. Blick, "Coherent superposition of photon- and phonon-assisted tunneling in coupled quantum dots," *Physical Review B*, vol. 64, no. 24, Article ID 241302, 4 pages, 2001.

[70] B. V. Kamenev, E.-K. Lee, H.-Y. Chang, et al., "Excitation-dependent photoluminescence in Ge/Si Stranski-Krastanov nanostructures," *Applied Physics Letters*, vol. 89, no. 15, Article ID 153106, 3 pages, 2006.

[71] C. J. Williams, E. Corbin, M. Jaros, and D. C. Herbert, "Auger recombination in strained Si_xGe_{1-x}/Si superlattices," *Physica B*, vol. 254, no. 3-4, pp. 240–248, 1998.

[72] E.-K. Lee, L. Tsybeskov, and T. I. Kamins, "Photoluminescence thermal quenching in three-dimensional multilayer SiSiGe nanostructures," *Applied Physics Letters*, vol. 92, no. 3, Article ID 033110, 3 pages, 2008.